

Toy nanoindentation model and incipient plasticity

I. Plans^{a,b}, A. Carpio^c, L. L. Bonilla^a

^a*G. Millán Institute for Fluid Dynamics, Nanoscience and Industrial Mathematics,
Universidad Carlos III de Madrid, 28911 Leganés, Spain.*

^b*Laboratoire des Colloïdes, Verres et Nanomatériaux, UMR 5587, Université Montpellier
II and CNRS, 34095 Montpellier, France.*

^c*Departamento de Matemática Aplicada, Universidad Complutense de Madrid, 28040
Madrid, Spain*

Abstract

A toy model of two dimensional nanoindentation in finite crystals is proposed. The crystal is described by periodized discrete elasticity whereas the indenter is a rigid strain field of triangular shape representing a hard knife-like indenter. Analysis of the model shows that there are a number of discontinuities in the load vs penetration depth plot which correspond to the creation of dislocation loops. The stress vs depth bifurcation diagram of the model reveals multistable stationary solutions that appear as the dislocation-free branch of solutions develops turning points for increasing stress. Dynamical simulations show that an increment of the applied load leads to nucleation of dislocation loops below the nanoindenter tip. Such dislocations travel inside the bulk of the crystal and accommodate at a certain depth in the sample. In agreement with experiments, hysteresis is observed if the stress is decreased after the first dislocation loop is created. Critical stress values for loop creation and their final location at equilibrium are calculated.

Email addresses: plans@lcvn.univ-montp2.fr (I. Plans), carpio@mat.ucm.es (A. Carpio), bonilla@ing.uc3m.es (L. L. Bonilla)

Key words: nanoindentation, dislocations, plasticity, defects, crystal lattices, nucleation

PACS: 82.40.Bj, 05.45.-a, 61.72.Bb

2000 MSC: 70K50, 65P30, 74A60, 65Z05

1. Introduction

Regularizations of continuum theories typically resolve the difficulties of the latter at small scales and often allow precise calculations and descriptions at these scales. This is the case of the Navier-Stokes equations which regularize the inviscid Euler equations of Fluid Mechanics (1), of the lattice regularizations of Quantum Field Theory and phase transitions (2), etc. Classical elasticity theory is unable to describe the nucleation and motion of crystal defects (3), dislocations (4), cracks (5; 6), phase boundaries (7), or more complex phenomena such as friction (8; 9; 10; 11). Lattice regularizations of elasticity can describe the structure and motion of nucleated defects and can be analyzed to extract qualitative and quantitative information about the phenomena at hand so as to provide a deep physical understanding (10; 6). In the case of dislocations, periodized discrete elasticity can describe depinning of dislocations at the Peierls stress (12), dislocation cores and dislocation interaction (13), stable defects corresponding to dislocations in graphene membranes and instability of Stone Wales defects (14; 15), and homogeneous nucleation of dipoles in a sheared lattice (16).

Metals usually contain a great number of dislocations whose motion, creation, annihilation and interaction are largely responsible for plastic behavior (4). Introducing defects in a crystal typically impedes dislocation motion

and multiplication thereby strengthening the material (strain hardening). At small length scales (such as those intervening in compression of thin whiskers), dislocations may leave the sample which results in its hardening via dislocation starvation (17) as observed in compression of nanopillars (18). Incipient plasticity occurs when defects are created in a hitherto perfect crystal by different means. Nanoindentation experiments are excellent ways to probe incipient plasticity (19; 20; 21; 22) and so are indentation experiments in colloidal crystals (23). In these experiments, the penetration depth inside the crystal is measured as the load on the indenter increases, which results in a discontinuous load versus depth diagram. The discontinuities in the diagram are thought to indicate dislocation nucleation inside the crystal. Different types of calculations have been used to interpret nanoindentation, ranging from atomistic simulations to continuum mechanics interpretations or combinations thereof (24; 25; 21; 26).

In this paper we present and analyze an atomistic toy model of nanoindentation to show that discontinuities in the load vs penetration length diagram do correspond to nucleation of dislocation loops ¹. We also use this model and its analysis to find different loading-unloading stress vs depth curves, in agreement with experimental observations (19). We have used the AUTO software (27) to find and numerically continue the branches of stationary

¹In a 2D model, dislocation dipoles are pairs of edge dislocations of opposite Burgers vectors with infinitely long extra half rows of atoms that go from the dislocation point outwards. Dislocation loops are pairs of edge dislocations with opposite Burgers vectors sharing a finite segment of extra atoms that join their respective dislocation points. See Figures 10 and 9 of (13).

configurations of our model starting from the perfect lattice. Thus we are able to calculate both *stable and unstable* stationary configurations and the bifurcation diagram (maximum strain/dimensionless stress F vs penetration depth δ), which is something that cannot be done using Molecular Dynamics (MD) simulations due to neighbor upgrading protocols. The bifurcation diagram exhibits multistability of stationary solutions whose configurations display an integer number of dislocation loops. Starting from the unstressed crystal and as F increases, δ increases until a turning point² is reached. As F surpasses a critical value F_c , a dislocation loop is nucleated and the profile evolves to that of the next stable solution branch in the bifurcation diagram (having a larger δ). This gives rise to a discontinuity in the load vs depth diagram for static solutions. Further increments of the load give rise to new discontinuities when successive turning points of the different stable solution branches are reached. In this simple model, nucleation of dislocation loops is a first order phase transition and hysteresis is possible: for $F > F_c$, there is an abrupt jump of δ due to dislocation loop nucleation and the unloading curve follows the second stable branch which has larger δ for the same F as in the loading curve. For our simple model, the second stable branch ends at a positive value of F . Further decrease thereof provokes reabsorption of the nucleated dislocation loop at the indenter tip and a sudden decrease of δ to its value on the elastic curve.

Our toy model is as follows. Consider a 2D simple cubic lattice with displacement vector measured in units of the lattice constant l , lattice points

²Points with zero or infinite slope where a branch of solutions changes from stable to unstable are turning points. See Fig. II.1 of (28).

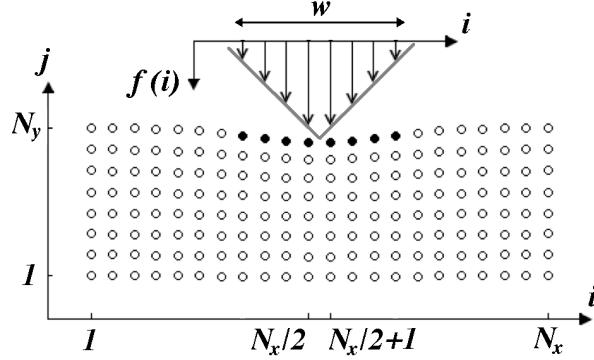


Figure 1: Modeling of a nanoindentation experiment. The stress field scales with the numerical continuation parameter F , such that the maximum downward vertical displacement at the central part of the upper surface satisfies $D_2^- v_{N_x/2, N_y} = -F$.

labelled by indices (i, j) , $i = 1, \dots, N_x$ and $j = 1, \dots, N_y$. The nanoindenter at the central region of the upper surface is a hard ‘knife’ represented by a fixed strain field which decreases linearly from zero to $-F$ and then increases to zero again, as depicted in Fig. 1. At the other boundaries, the displacement vector is zero. The indenter may cause gliding of atom columns in the vertical direction and therefore the displacement vector changes more in the vertical direction than in the horizontal one. Then a simple displacement vector $(0, v_{i,j})$ captures the qualitative features of the physical system. It is convenient to use coordinates (x, y) with $x = i - (N_x + 1)/2$ and $y = j - (N_y + 1)/2$ whose origin is the lattice center. The displacements obey the following nondimensional equations:

$$m \frac{d^2 v_{i,j}}{dt^2} + \alpha \frac{dv_{i,j}}{dt} = v_{i,j+1} - 2v_{i,j} + v_{i,j-1} + A [g_a(v_{i+1,j} - v_{i,j}) + g_a(v_{i-1,j} - v_{i,j})], \quad (1)$$

where $g_a(x)$ is a one-parameter family of periodic functions of x with period

$$g_a(x) = \frac{2a}{\pi} \begin{cases} \sin\left(\frac{\pi x}{2a}\right), & -a \leq x \leq a, \\ \sin\left(\frac{\pi(x-1/2)}{2a-1}\right), & a \leq x \leq 1-a, \end{cases} \quad (2)$$

and $0 < a < 1/2$, such that $g_a(x) \sim x$ as $x \rightarrow 0$ (see below for motivation).

The boundary conditions are

$$D_2^- v_{i,N_y} \equiv v_{i,N_y} - v_{i,N_y-1} = -F f(i), \quad (3)$$

$$v_{i,j} = 0, \quad \text{if either } j = 1, i = 1, \text{ or } i = N_x. \quad (4)$$

For a symmetric and centered sharp indenter as depicted in Fig. 1 with an even number of atoms, w , and for even N_x , we have

$$f(i) = \frac{2}{w} \times \begin{cases} i - \frac{N_x-w}{2}, & \frac{N_x-w}{2} + 1 \leq i \leq \frac{N_x}{2}, \\ \frac{N_x+w}{2} + 1 - i, & \frac{N_x}{2} + 1 \leq i \leq \frac{N_x+w}{2}, \\ 0, & \text{otherwise.} \end{cases} \quad (5)$$

This indenter has a rectangular cross section $S = Lwl$, $wl \ll L$, where l is the lattice constant and L is the length of the knife. A more realistic modeling of the knife would require considering horizontal displacements which we are ignoring in our model. Note that $f(N_x/2) = f(1 + N_x/2) = 1$ and that $\sum_i f(i) = 1 + w/2$. In Eq. (1), $A = C_{44}/C_{11}$ provided we consider cubic crystals with elastic constants C_{11} , C_{12} , C_{44} . The vertical component of the stress tensor σ_{22} is simply $C_{11} D_2^- v_{i,j}$ in our model, and therefore the strain at the surface given by Eq. (3) is also the nondimensional applied stress σ_{22}/C_{11} . We also have $\sigma_{21}/C_{11} = A g_a(D_1^- v_{i,j})/2$. The relation between the stress at the surface and an applied load P is

$$P = \frac{S}{w} \sum_{i=2}^{N_x} \sin \varphi(i) \sigma_{21}(i, N_y) - \frac{S}{w} \sum_{i=2}^{N_x} \cos \varphi(i) \sigma_{22}(i, N_y),$$

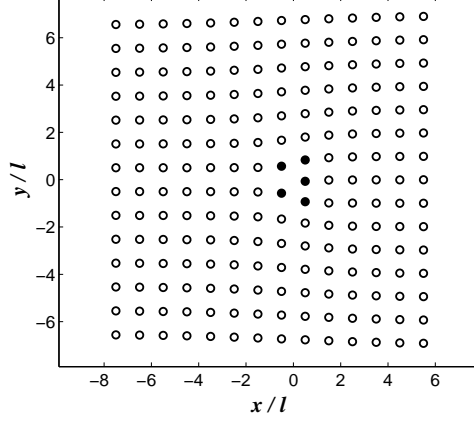


Figure 2: An edge dislocation parallel to the z axis with Burgers vector $(0, -1)$.

where $\varphi(i)$ is the angle between the normal to the indenter surface and the y axis, with $\tan \varphi = D_1^- v_{i,N_y}$. We obtain

$$\Lambda \equiv \frac{P}{C_{11}S} = \frac{F}{w} \sum_{i=2}^{N_x} \cos \varphi(i) f(i) + \frac{A}{2w} \sum_{i=2}^{N_x} \sin \varphi(i) g_a(D_1^- v_{i,N_y}), \quad (6)$$

which relates the nondimensional load Λ to the stress F . If we select a nondimensional time scale $C_{11}t/(\rho l^2 \gamma) \rightarrow t$, then $\alpha = 1$ and $m = C_{11}/(\rho l^2 \gamma^2)$, where γ is a friction coefficient with units of frequency, ρ is the mass density and $v_{i,j}$ is measured in units of l . With this choice of scales, we can consider the overdamped case with $m = 0$. On the other hand, if we select a nondimensional time scale $C_{11}^{1/2}t/(l\rho^{1/2}) \rightarrow t$, then $m = 1$ and $\alpha = l\gamma\sqrt{\rho/C_{11}}$. With this second choice of scales, we can consider the conservative case with $\alpha = 0$.

If $g_a(x) = x$ in Eq. (1), we obtain discretized scalar linear elasticity. Why do we have to use the periodic functions (2)? To allow atoms change neighbors during dislocation motion. The fact that the functions (2) are

periodic allows the atoms to change neighbors while the computational grid remains unchanged (and so the dynamical system (1) whose linear stability will be analyzed).

Let us explain this idea. Assume that we have an extra half row of atoms in the square lattice that is parallel to the positive x direction (edge dislocation with Burgers vector $(0, -1)$), as depicted in Fig. 2. If these atoms move one step downwards and occupy the equilibrium positions of their neighboring atoms, the latter are displaced downwards and become the extra half row representing the edge dislocation that has therefore moved one step downwards. If these new atoms move one step downwards in the same way, a new half row replaces them and the dislocation has moved another step. During this glide motion, the leftmost atom in the half row changes neighbors horizontally and only once whereas all the other atoms in the half row continue having the same neighbors. Even though the dislocation can glide for a long distance, single atoms move very little and only a very small fraction of these atoms change neighbors. Instead of updating neighbors during glide motion, we can construct a periodized discrete elasticity model by using a nonlinear periodic function g_a in (1), with period equal to the lattice space and $g_a(x) \sim x$ as $x \rightarrow 0$. A simple example is (2). This model changes neighbors without updating, thereby allowing atomic half rows to glide in the y -direction.

As the applied stress becomes sufficiently large, there appear edge dislocation loops whose Burgers vectors are directed along the y axis. Gliding along other directions is not possible in this model: we would need a two-component displacement vector and a periodic function of discrete differences

along the x axis (13). The parameter a controls the asymmetry of g_a : a increases, the interval over which $g'_a(x) > 0$ increases at the expense of the interval over which the slope of g_a is negative. As a increases, the (dimensionless) Peierls stress σ_p needed for a dislocation to start moving increases whereas the size of the dislocation core and its mobility both decrease (13)³. The value of a can be selected so that the Peierls stress calculated from (1) fits values measured in experiments or calculated using MD. Namely, for a 16×30 lattice with $A = 0.2258$ (corresponding to gold) we get $\sigma_p = 0.004$ for $a = 0.2$ compared to $\sigma_p = 0.03$ for $a = 0.4$.

In the symmetric case $a = 1/4$, (1) and (2) are the governing equations of the interacting atomic chains model (29).

2. Methodology and Results

We consider parameters $A = 0.2258$ (gold), $a = 0.2$, for a 22×42 lattice and a four atom indenter, $w = 4$. Similar results were obtained when the same indenter is placed in the center of the upper surface of other lattices with even N_x and N_y . Asymptotically stable stationary solutions of the model equations (1) with boundary conditions (3) - (4) are obtained by numerically solving the equations with appropriate initial conditions and overdamped dynamics, $m = 0$, $\alpha = 1$. For conservative dynamics, $m = 1$, $\alpha = 0$, the same stationary solutions are stable but not asymptotically stable. Unstable solutions are unstable no matter which dynamics is considered.

At zero applied load the perfect lattice is found. As the dimensionless

³Note that the parameter α used in (13) corresponds to $-a + 1/2$ in (2) and therefore the Peierls stress in Figure 2 of (13) decreases as α increases.

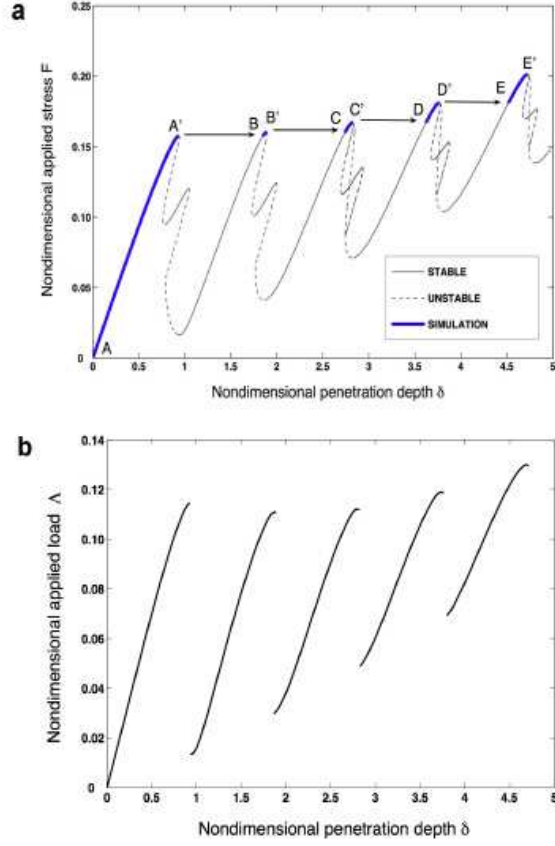


Figure 3: (a) Maximum vertical nondimensional stress F *vs* nondimensional indenter penetration depth δ obtained by numerical continuation of the stationary solution at $F = \delta = 0$ for a 16×42 lattice, with $A = 0.2258$ (gold), $a = 0.2$. By increasing adiabatically F from zero, we sweep this bifurcation diagram following the path $A \rightarrow A' \rightarrow B \rightarrow B' \rightarrow C \rightarrow C' \rightarrow D \rightarrow D' \rightarrow E \rightarrow E'$. (b) Similar diagram of nondimensional applied load *vs* nondimensional penetration depth. Only the long stable portions of the bifurcation diagram are shown.

applied load F increases from zero, we can monitor the penetration depth of the indenter,

$$\delta = -\frac{1}{w} \sum_{i=1+(N_x-w)/2}^{(N_x+w)/2} v_{i,N_y-1}, \quad (7)$$

and obtain the relation between F and δ . We have used the AUTO software (27) to find and numerically continue the branches of stationary solutions of our model starting from the perfect lattice with $F = 0$, $\delta = 0$. The results are represented in Fig. 3a, whereas Fig. 3b shows the corresponding load vs penetration depth diagram (in dimensionless units). The bifurcation diagram shows a connected branch of stationary solutions which begins at the origin (marked with A in Fig. 3a). Each point of the long stable portions of this branch corresponds to a single configuration of the lattice. There are many turning points (local maxima or minima, some of them indistinguishable at the scale of the plot) connecting stable and unstable regions. The main turning points point out to the occurrence of different nucleation events, which we shall now describe.

The longest stable portions of the stationary branch end at turning points A' , B' , C' , D' and E' in increasing order of δ (solid lines in Fig. 3a). The corresponding configurations have 0, 1, 2, 3 and 4 dislocation loops, respectively, as shown in Figs. 4a, c and e. We may call AA' the dislocation-free *elastic branch*, whereas the other long stable portions of Fig. 3a signal the beginning of plasticity due to loop formation. The component $e_{1,2} = g_a(v_{i+1,j} - v_{i,j})/2$ of the strain field (proportional to the dimensionless shear stress) provides a good visualization of the dislocation loops as Figures 4b, d and f show. Each loop comprises two dislocations whose cores are located at points with

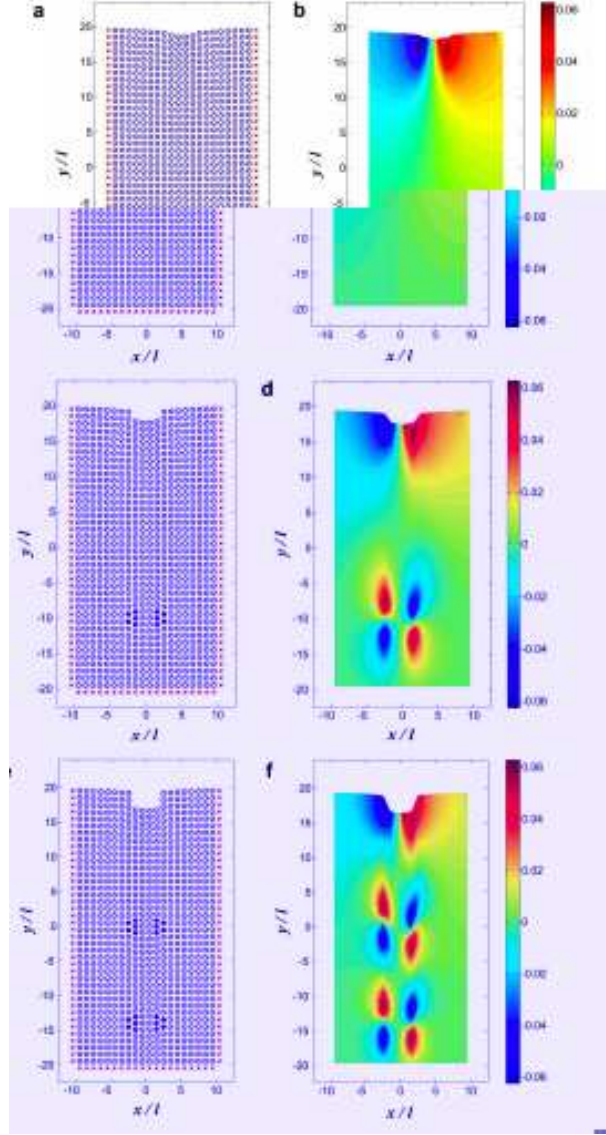


Figure 4: Stable configurations at the turning points (a) A' , (c) B' and (e) C' of the bifurcation diagram in Fig. 3. Panels (b), (d) and (f) visualize the component $e_{1,2} = g_a(v_{i+1,j} - v_{i,j})/2$ of the strain tensor corresponding to A' , B' and C' , respectively.

$i = 1 + (N_x - w)/2$ and $i = (N_x + w)/2$ below the indenter. Using the lattice constant as unit of length, the first dislocation is at the column $i = 1 + (N_x - w)/2$ and it has Burgers vector $(0, -1)$, whereas the second dislocation is located at the column $i = (N_x + w)/2$ and it has Burgers vector $(0, 1)$.

Note that after some of its turning points the solution branch bends over itself, and connects back to earlier limit points (C' , D' , E' in Fig. 3a) by means of unstable portions. To each point of the short stable portions found after these limit points, there correspond two lattice configurations, which are symmetrical with respect to $x = 0$. They contain one extra edge dislocation in addition to the dislocation loops that the configuration corresponding to the preceding long stable portion with smaller δ may contain. In one configuration, the dislocation point of the extra dislocation with Burgers vector $(0, 1)$ is located at $i = (N_x + w)/2$, at some distance below the indenter (as occurs in the short stable portions after A' and B'). The other configuration has a dislocation point on the same row, with opposite Burgers vector $(0, -1)$, which is located at $i = 1 + (N_x - w)/2$. As it will be explained later, these short stable portions are not reached by any of our dynamical experiments. However, if the configurations corresponding to unstable branches are depicted, nucleation or disappearance of the extra edge dislocation is observed as we run AUTO along the unstable branch towards the turning point where it joins a stable branch.

3. Adiabatic sweeping of the bifurcation diagram

By increasing adiabatically F from $F = 0$ (up-sweep), the stable portions AA' , BB' , CC' , DD' , EE' of the solution branch in the bifurcation diagram of Fig. 3a are successively swept. A' marks the critical value F_c above which dislocation loops are nucleated. B' , C' , D' and E' are the last points found in the corresponding stable portion of the solution branch before a new dislocation loop is nucleated and a jump to another stable portion occurs during adiabatic up-sweep. At these points, with stresses $F_{A'}$, $F_{B'}$, $F_{C'}$, $F_{D'}$ and so on, δ jumps to the corresponding value in the next branch, as indicated by the arrows in Fig. 3a, and a new dislocation loop is formed. What is observed during slow up-sweep by numerically solving (1)? After F surpasses $F_{A'}$ in Fig. 3a with configuration as in Fig. 4a, a dislocation loop is nucleated *immediately below the indenter tip* and it glides downwards until it reaches its stable position inside the sample at $y/l = -10$ (configuration B). The jump $A' \rightarrow B$ in Fig. 3a has taken place. By adiabatically increasing F , we may reach B' (cf. Fig. 4c and d), which is almost identical to B . After F surpasses $F_{B'}$, a new dislocation loop is nucleated at the indenter tip, and now both loops glide downwards until they reach their respective stable positions $y/l = 0, -14$ in configuration C . Further increase of F leads to configuration C' (see Fig. 4e). Additional up-sweep repeats this pattern: old dislocation loops glide downwards and new ones appear beside the indenter tip.

If we start relaxing adiabatically the load on the nanoindenter after F has reached F_B , then the displacement δ does not go back to the value $\delta_{A'}$. Instead, its value decreases following the stable branch containing the point (δ_B, F_B) in Fig. 3a. As F decreases, the loop created in the middle of the

sample glides upwards towards the indenter until the turning point with lowest value of F is reached. At this stable configuration, the loop is located at $y/l = 5$. An additional decrease of the load results in a downward jump to the elastic solution branch. During this dynamical process, the dislocation loop glides upwards and disappears as it reaches the indenter (in 3D loops may be anchored due to cross-slip or to preexisting defects (3)). In a standard model of plastic behavior, we would expect that the second stable branch of stationary solutions extend to $F = 0$, $\delta > 0$ without losing the dislocation loop.

There are other stable portions of the stationary solution branch in Fig. 3a that cannot be reached by up- or down-sweeping the bifurcation diagram: the short portions with intermediate values of δ between those of two long stable portions.

4. Results for other parameter values

For the same values of a and A , we have changed the position of the indenter, made it wider, changed the size of the lattice or considered odd N_x . In all these cases, the F (or Λ) vs δ diagram is similar to that in Fig. 3, as shown in Fig. 5 for a lattice of different size. The unstable portions of the bifurcation diagram change although not the long stable portions, and therefore the responses to adiabatic up- and down-sweeping the diagram are the same. For parameter values corresponding to the point B' , the dislocation loop is located at a height roughly two thirds of N_y ⁴. However there are some

⁴For $N_x = 16$, $\delta_{B'}/N_y = 0.625, 0.661$ and 0.668 for $N_y = 30, 42$ and 58 , respectively.

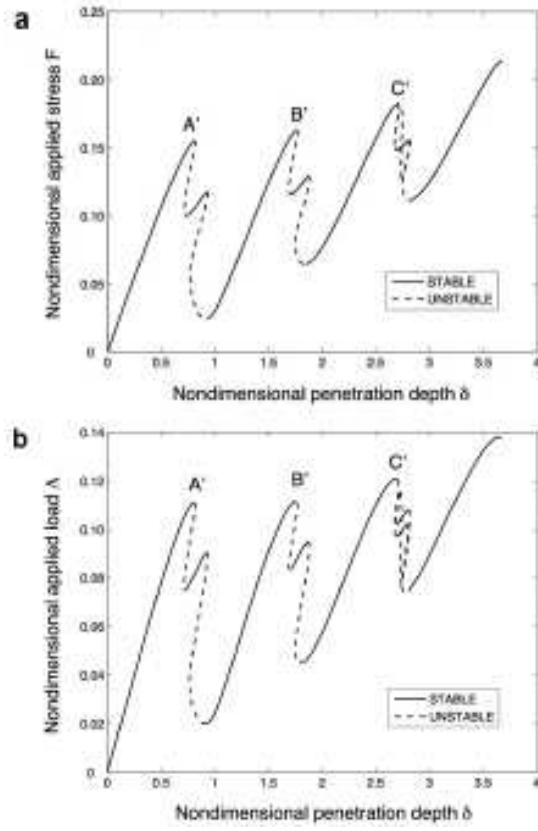


Figure 5: Same as in Fig. 3 for a 16x30 lattice.

differences worth noticing. For a 22×42 lattice, increasing the indenter width from $w = 4$ to $w = 10$ increases only slightly $F_{A'}$, from 0.1575 to 0.1598, but now the cavities created by the indenter are not rectangular as in Fig. 4. Instead, they exhibit steps which made them triangular in shape. Similar results are found for odd N_x when the maximum $f(i)$ is reached at only one atom, $i = [N_x/2]$. For a 17×30 lattice with $w = 5$, the bifurcation diagrams are similar and triangular cavities are observed. A shorter indenter with $w = 4$ placed on atoms 7, 8, 9 and 10 of a 17×30 lattice again gives rise to bifurcation diagram similar to Fig. 5 but now some of the short intermediate stable portions having one extra unpaired edge dislocation can be distinguished in the diagram because their corresponding configurations are no longer symmetric. Actually, it is not always after the third turning point (C' in Figs. 3 and 5) that these short intermediate stable portions correspond to two solutions. We find that for a 22×22 lattice it occurs after the second turning point, B' . If we use $A = 0.448$ (corresponding to copper), for a 16×30 lattice the results are qualitatively similar to those so far presented except that: (i) the point A' has a larger $F = 0.2191$ and a smaller $\delta = 0.7958$ (compared to $F = 0.1553$ and $\delta = 0.8128$ for gold in Fig. 5); and (ii) close to the minima of the bifurcation diagram, the branch of stationary solutions is wiggly with several turning points separating alternating stable and unstable solutions. These wiggly portions are also present in Fig. 5 but they are not visible at the scale chosen in the figure.

As mentioned before, augmenting a in Eq. (2) increases $F_{A'}$ and the Peierls stress and reduces the size of defect cores. For a 16×30 lattice with $w = 4$, $A = 0.2258$ (gold) and $a = 0.4$, we get $F_{A'} = 0.2558$, $\delta_{A'} = 1.2283$

(compared to $F = 0.1553$ and $\delta = 0.8128$ for $a = 0.2$) and it is quite hard to move dislocations (the dimensionless Peierls stress is $\sigma_p = 0.03$, compared to $\sigma_p = 0.004$ for $a = 0.2$). The bifurcation diagram changes in that the number of turning points increases enormously. However, the stable portions of the diagram have the same configurations and interpretations as those in Figs. 3 and 5. Then up-sweeping the diagram produces the same sequence of discontinuities due to formation of dislocation loops.

5. Conclusion

We have presented a toy model of 2D nanoindentation and incipient plasticity in a dislocation-free crystal based on periodized discrete elasticity. Analysis and numerical simulation of the model confirm that the discontinuities in the diagram of stress (or load) vs penetration depth are associated with the nucleation of dislocation loops (if stress is adiabatically increased) or with their absorption in contact with it (if stress is adiabatically decreased). Our simulations and analysis of the bifurcation diagram of solutions show that hysteresis occurs, leading to unloading curves which are different to the loading ones, in agreement with experimental observations. The analysis of the results obtained with AUTO yields the critical stress for dislocation nucleation, the type thereof and the depth at which dislocation loops are accommodated in their equilibrium positions.

Acknowledgments

We thank O. Rodríguez de la Fuente and J.M. Rojo for fruitful discussions and useful comments. This work has been supported by the Spanish Ministry

of Science and Innovation grants FIS2008-04921-C02-01 (LLB and IP) and FIS2008-04921-C02-02 (AC), by the Autonomous Region of Madrid under grant S-0505/ENE/0229 (COMLIMAMS) (LLB and IP) and by CM/UCM 910143 (AC).

References

- [1] Landau LD and Lifshitz EM. Fluid Mechanics (2nd ed.): Pergamon P., New York; 1987.
- [2] Amit DJ and Martín Mayor V. Field Theory, the Renormalization Group and Critical Phenomena (3rd. rev. ed.): World Sci. Singapore; 2005.
- [3] Hull D and Bacon DJ. Introduction to Dislocations (4th ed.): Butterworth-Heinemann, Oxford UK; 2001.
- [4] Hirth JP, Lothe J. Theory of Dislocations (2nd ed.): John Wiley and Sons, New York; 1982.
- [5] Slepian LI. Models and Phenomena in Fracture Mechanics: Springer, Berlin 2002.
- [6] Pla O, Guinea F, Louis E, Ghaisas SV and Sander LM. Straight cracks in dynamic brittle fracture. Phys Rev B 2000;61:11472-11486.
- [7] Zhen Y and Vainchtein A. Dynamics of steps along a martensitic phase boundary I: Semi-analytical solution. J Mech Phys Solids 2008;56:496-520.

- [8] Rubinstein SM, Cohen G and Fineberg J. Detachment fronts and the onset of dynamic friction. *Nature* 2004;430(7003):1005-1009.
- [9] Marder M. Friction - Terms of detachment. *Nature Materials* 2004;3(9):583-584.
- [10] Gerde E and Marder M. Friction and fracture. *Nature* 2001;413(6853),285-288.
- [11] Kessler DA. Surface physics - A new crack at friction. *Nature* 2001;413(6853),260-261.
- [12] Carpio A and Bonilla LL. Edge dislocations in crystal structures considered as traveling waves in discrete models. *Phys Rev Lett* 2003;90:135502.
- [13] Carpio A and Bonilla LL. Discrete models of dislocations and their motion in cubic crystals. *Phys Rev B* 2005;71(13):134105.
- [14] Carpio A, Bonilla LL, de Juan F and Vozmediano MAH. Dislocations in graphene. *New J Phys* 2008;10:053021.
- [15] Carpio A, Bonilla LL. Periodized discrete elasticity models for defects in graphene. *Phys Rev B* 2008;78(8):085406.
- [16] Plans I, Carpio A and Bonilla LL. Homogeneous nucleation of dislocations as bifurcations in a periodized discrete elasticity model. *Europhys Lett* 2008;81(3):36001.
- [17] Greer JR and Nix WD. Nanoscale gold pillars strengthened through dislocation starvation. *Phys Rev B* 2006;73(24):245410.

- [18] Shan ZW, Mishra RK, Asif SAS, Warren OL and Minor AM. Mechanical annealing and source-limited deformation in submicrometre-diameter Ni crystals. *Nature Materials* 2008;7(2):115-119.
- [19] Lorenz D, Zeckzer A, Hilpert U, Grau P, Johansen H and Leipner HS. Pop-in effect as homogeneous nucleation of dislocations during nanoindentation. *Phys Rev B* 2003;67(17):172101.
- [20] Asenjo A, Jaafar M, Carrasco E and Rojo JM. Dislocation mechanisms in the first stage of plasticity of nanoindented Au(111) surfaces. *Phys Rev B* 2006;73(7):075431.
- [21] de la Fuente OR, Zimmerman JA, González MA, de la Figuera J, Hamilton JC, Pai WW and Rojo JM. Dislocation emission around nanoindentations on a (001) fcc metal surface studied by scanning tunneling microscopy and atomistic simulations. *Phys Rev Lett* 2002;88(3):036101.
- [22] Navarro V, de la Fuente OR, Mascaraque A and Rojo JM. Uncommon Dislocation Processes at the Incipient Plasticity of Stepped Gold Surfaces. *Phys Rev Lett* 2008;100(10):105504.
- [23] Schall P, Cohen I, Weitz DA and Spaepen F. Visualizing dislocation nucleation by indenting colloidal crystals. *Nature* 2006;440(7082):319-323.
- [24] Bulatov VV and Cai W. Computer simulations of dislocations: Oxford University Press, Oxford, UK; 2006.

- [25] Kelchner CL, Plimpton SJ and Hamilton JC. Dislocation nucleation and defect structure during surface indentation. *Phys Rev B* 1998;58(17):11085-11088.
- [26] Zhu T, Li J, Van Vliet KJ, Ogata S, Yip S and Suresh S. Predictive modeling of nanoindentation-induced homogeneous dislocation nucleation in copper. *J Mech Phys Solids* 2004;52(3): 691-724.
- [27] Doedel EJ, Paffenroth RC, Champneys AR, Fairgrieve TF, Kuznetsov YA, Oldeman BE, Sandstede B and Wang X. AUTO2000: Continuation and bifurcation software for ordinary differential equations (with HomCont). Technical Report, Concordia University; 2002. <https://sourceforge.net/projects/auto2000/>, <http://indy.cs.concordia.ca/auto/>
- [28] Iooss G and Joseph DD. *Elementary Stability and Bifurcation Theory*: Springer, New York; 1980.
- [29] Landau AI. Application of a model of interacting atomic chains for the description of edge dislocations. *Phys Status Solidi B* 1994;183(2),407-417.